Molecular Modeling of a Functionalized Aib-Based Octapeptide by Molecular Mechanics Calculations Restrained by NMR and Fluorescence Data in DMSO

B. Pispisa,*,† A. Palleschi,‡ M. E. Amato,§ A. L. Segre,|| and M. Venanzi†

Dipartimento di Scienze e Tecnologie Chimiche, Università di Roma Tor Vergata, 00133 Roma, Italy, Dipartimento di Chimica, Università di Roma La Sapienza, 00185 Roma, Italy, Dipartimento di Scienze Chimiche, Università di Catania, 95125 Catania, Italy, and C.N.R. Area della Ricerca di Roma, 00016 Monterotondo Scalo (Roma), Italy

Received December 12, 1996; Revised Manuscript Received May 19, 1997[⊗]

ABSTRACT: The structural features of the sequential octapeptide Boc-$(Leu)_2$-Lys(P)-$(Aib)_2$-$(Leu)_2$-Lys-(N)-OtBu, where P is protoporphyrin IX and N is naphthalene, were investigated in DMSO by NMR and fluorescence spectroscopy. Earlier IR, CD, and fluorescence results showed that this compound attains a 3_{10}-helical conformation in methanol or water/methanol (75/25, v/v). By contrast, the backbone structure in DMSO is destroyed, but the high helix propencity of the Aib residues forces the peptide to attain locally ordered arrangements, reminiscent of β-turn features. Both NMR coupling constant and NOE connectivity data allowed us to compute the structural features of part of the molecule, but only their combination with fluorescence results allowed us to build up the whole molecular model. Implications of fluorescence data on the dynamics of internal rotation of the chromophores are briefly discussed.

Introduction

Despite the idea that peptides shorter than, say, 10−12 amino acids are generally devoid of structure and assume random conformations,[1] we have recently shown that linear peptides formed by 6−10 amino acids, of general formula Boc-$(Leu)_2$-Lys(P)-$(AA)_n$-$(Leu)_2$-Lys(N)-OtBu, where $n = 0-4$, N = naphthalene, P = protoporphyrin IX, and AA = Ala or Aib, are able to attain ordered structures in methanol or water/methanol (75/25, v/v) solution.[2,3] By combining fluorescence data with both IR and CD spectral results, we were able to prove that the backbone chain of P$(Ala)_n$N peptides populates α-helical conformations, the more the longer the backbone, while that of P$(Aib)_n$N attains 3_{10}-helical structures,[3] in agreement with the proven ability of Aib to form 3_{10}-helices in solution, owing to the steric constraints of the *gem*-dimethyl groups.[4] Interestingly enough, the corresponding blanks show that only $(Aib)_n$N behaves as P$(Aib)_n$N, while $(Ala)_n$N peptides are in a random coil, whatever the length of the backbone chain.

To ascertain whether the high helix propencity of Aib holds even in destructuring solvents, such as DMSO, we performed a thorough investigation on the structural features of the P$(Aib)_2$N octapeptide in this solvent. We present here the results of this study, based on ^{1}H-NMR and fluorescence data, suggesting the presence of two families of structures, both characterized by locally ordered arrangements, reminiscent of β-turn features. A further aim of the paper was to show how only the combination of the structural information from both NMR and fluorescence experiments in DMSO allowed us to compute the entire molecular structure of the sterically most favorable conformers of P$(Aib)_2$N.

Experimental Section

The abbreviations used for the amino acids follow the Recommendations of the IUPAC-IUB Commission of Biochemical Nomenclature. The other abbreviations used throughout the paper are the following: COSY, double quantum filtered correlated spectroscopy; DMSO, dimethyl sulfoxide; NOE, nuclear Overhauser effect; NOESY, nuclear Overhauser enhancement spectroscopy; TOCSY, total correlation spectroscopy; TMS, tetramethylsilane; TPPI, time proportional phase incrementation.

Materials. P$(Aib)_2$N octapeptide and the corresponding blanks, $(Aib)_2$N and $(Aib)_2$P, depending on the bound chromophore, are formed by two Leu-Leu-Lys triads, linked together through two Aib residues. Both monomeric and cross-linked dimeric protoporphyryl peptides were synthesized, but only the monomeric species will be reported here. The synthesis of the octapeptides was already reported.[2,3]

DMSO-d_6 (99.95% isotopic purity) for NMR measurements was purchased from Aldrich, and the other spectroscopically pure solvents were purchased from Merck.

Methods. ^{1}H-NMR spectra were obtained at 300 K on a Bruker AMX 600 instrument operating at 600.13 MHz. The sample was dissolved in DMSO-d_6, in concentration around 2 mg/mL, no special precautions being taken to reduce the size of the water peak in the solvent. No significant variation in shifts or line broadening was observed on varying peptide concentration. 1-D ^{1}H spectra were acquired in 32K data points, with a spectral width of 18 ppm (−4.5−13.5 ppm).

COSY,[5] TOCSY,[6] and NOESY[7] spectra were acquired using standard procedures in the phase sensitive mode, by the TPPI method.[8] The chemical shifts were referenced to TMS but were measured from DMSO assumed at 2.500 ppm. The COSY, 2-D TOCSY, and NOESY spectra were acquired with 64 transients of 1K data points in f_2. The 2-D TOCSY experiments were run using the MLEV17 spin-locking sequence for isotropic mixing following the procedure of Bax.[9] A mixing time of 100 ms and 80 cycles of a MLEV17 sequence with a spin-locking field of 12 kHz were employed. The recycle delay was 2 s. NOESY spectra were recorded with a mixing time of 200 ms.

In all 2-D experiments, 512 increments were used, and the data sets were zero-filled to 1K in f_1 before Fourier transformation. Various Gaussian and sine bell weighted functions were applied in each dimension, and no spectrum was symmetrized.

Both steady-state and time-resolved fluorescence experiments were performed at room temperature with an Edinburgh CD900 instrument, as already reported.[2] The solutions were previously bubbled for about 20 min with ultrapure nitrogen. The decay curves were fitted by a nonlinear least-squares analysis to exponential functions by an iterative

† Università di Roma Tor Vergata.
‡ Università di Roma La Sapienza.
§ Università di Catania.
|| C.N.R. Area della Ricerca di Roma.
⊗ Abstract published in *Advance ACS Abstracts,* July 1, 1997.

S0024-9297(96)01833-5 CCC: $14.00

Table 1. NOE Contacts and Coupling Constants from NMR Measurements on $(Aib)_2N$ (A) and $P(Aib)_2N$ (B) Octapeptides in DMSO at 300 K

amino acid	d_{NN}[a]	$d_N{}^{\alpha}$[b]	$J_N{}^{\alpha}{}_H$
	A. Boc-Leu[1]-Leu[2]-Lys[3]-Aib[4]-Aib[5]-Leu[6]-Leu[7]-Lys[8](N)-OtBu		
Leu[1]			7.0−7.6
Leu[2]	Leu[1]−Lys[3]	Leu[1]	7.0−8.0
Lys[3]		Leu[2]	≈5.0
Aib[4]	Lys[3]	Lys[3]	
Aib[5]	Aib[4]		
Leu[6]			7.2
Leu[7]		Leu[6]	9.0
Lys[8]	Leu[6]−Leu[7]	Leu[7]	8.0−9.0
	B. Boc-Leu[1]-Leu[2]-Lys[3](P)-Aib[4]-Aib[5]-Leu[6]-Leu[7]-Lys[8](N)-OtBu		
Leu[1]			7.8
Leu[2]	Leu[1]	Leu[1]	8.3
Lys[3]		Leu[2]	8.2
Aib[4]		Lys[3]	
Aib[5]	Leu[1]		
Leu[6]			8.7−8.9
Leu[7]		Leu[6]	8.3
Lys[8]	Leu[7]	Leu[7]	7.6−8.8

[a] d_{NN}: NOE contacts between NH_j ($j > i$) and NH_i. [b] $d_N{}^{\alpha}$: NOE contacts between NH_{i+1} and $C^{\alpha}H_i$.

deconvolution method. The distribution analysis of time decays was also performed.

Absorption spectra were recorded on a Jasco 7850 apparatus.

Results and Discussion

^{1}H-NMR Data. The effect of the bulkiness of the protoporphyrin chromophore on the NMR spectra was preliminarily afforded by investigating the spectral patterns of $P(Aib)_2N$ and $(Aib)_2N$. As a result, the NMR spectra of both octapeptides were comparable, in the sense that both spectral patterns show the occurence of several resonances due to rotational isomers whose interconversion is slow on the NMR time scale, as illustrated in Table 1. This rules out a specific effect of the porphyrin moiety on the detected signals.

We next investigated the amino acids' proton resonances, following the standard practice.[10,11] The absence of an H^{α} proton in Aib forced us to stop the sequential assignment for this part of the molecule. However, NOE cross-peaks between the methyl groups of Aib[5] and Aib[6] and $C^{\alpha}H$ and $C^{\beta}H$ of the closest amino acid residues allowed us to overcome any ambiguity in the complete identification of the backbone chain of the peptide. Figures 1−3 show the NH−$C^{\alpha}H$ spectral region in the NOESY experiments and the region of the TOCSY experiment, containing cross-peaks between the backbone amide protons and the aliphatic protons, respectively. In spite of the severe overlapping of the signals detectable in the proton spectra, the spin system of each residue in the backbone was distinguishable. On the other hand, the naphthalene chromophore linked to ϵ-N of the Lys[8] residue shows characteristic patterns of proton signals in the low-field region, being thus easily assignable, as are the signals of the protoporphyrin moiety bound to the ϵ-N of the Lys[3].

The characteristic patterns of cross-peaks between the backbone amide protons provide information about possible secondary structures. Either intra- or interresidue NOE cross-peaks involving backbone atoms were observed in the NOESY spectra, but the absence of NH−NH cross-peaks strongly suggests the lack of ordered conformations, either α-helix or 3_{10}-helix. Moreover, the ratio of the intensities of the sequential NOE

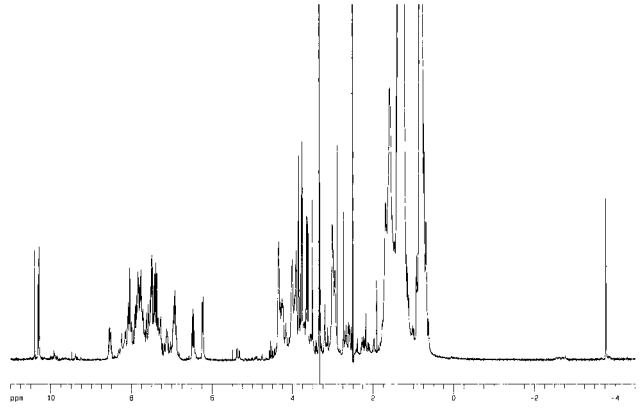

Figure 1. 1D ^{1}H-NMR spectrum at 600.13 MHz of $P(Aib)_2N$ in DMSO, showing the complex multiplicity due to the presence of different conformers in slow interconversion on the NMR time scale.

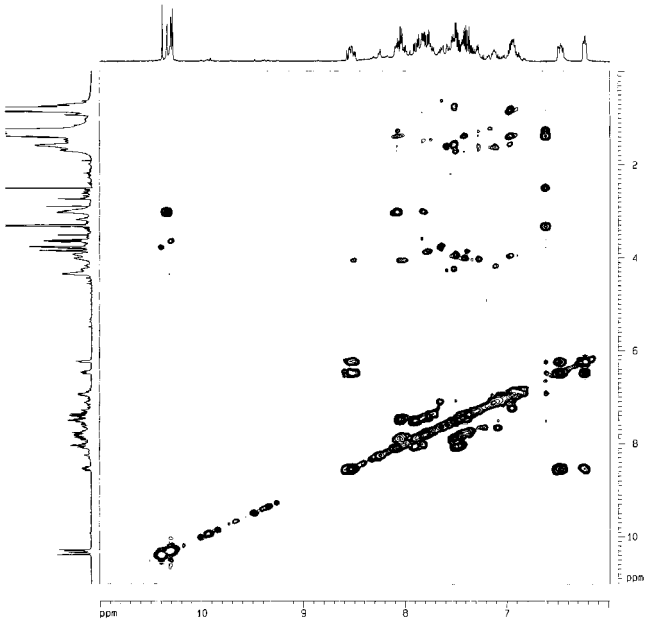

Figure 2. TOCSY map of $P(Aib)_2N$. In the F1 dimension the 0−10 ppm range is shown, while, for the sake of clarity, in the F2 dimension only the lower half of the spectrum is reported. The upfield porphyrinic NH is a singlet, so that its resonance was not included in the TOCSY experiment.

arising from NH−$C^{\alpha}H(i,i+1)$ over those of the intraresidue NOE corresponding to NH−$C^{\alpha}H(i,i)$ differs markedly for different secondary structures.

A further indication of the absence of helical structures in the solution is given by the finding that all the intraresidue NH−$C^{\alpha}H(i,i)$ NOE connectivities, not overlapped with other signals, are much weaker than the corresponding sequential ones, while in the case of a helical conformation the intraresidue NOE would be approximately five times stronger than the sequential NOE.

All these features lend plausibility to the idea that $P(Aib)_2N$ attains extended chain structures with connectivities roughly equivalent to those observed for single strands of β-sheet. In fact, the coupling constants for NH−$C^{\alpha}H(i,i)$ of this peptide, by analysis of the line splitting in the 1-D spectra of nonoverlapped signals, are around 8−9 Hz, as shown in Table 1, which are inconsistent with the α-helical conformation but are similar to those of β-sheet structures ($^3J_{NH-C\alpha_{H(i,i)}} \approx 9.0$ Hz [11]). These results, together with the NOE contacts reported in the same table, support the idea that

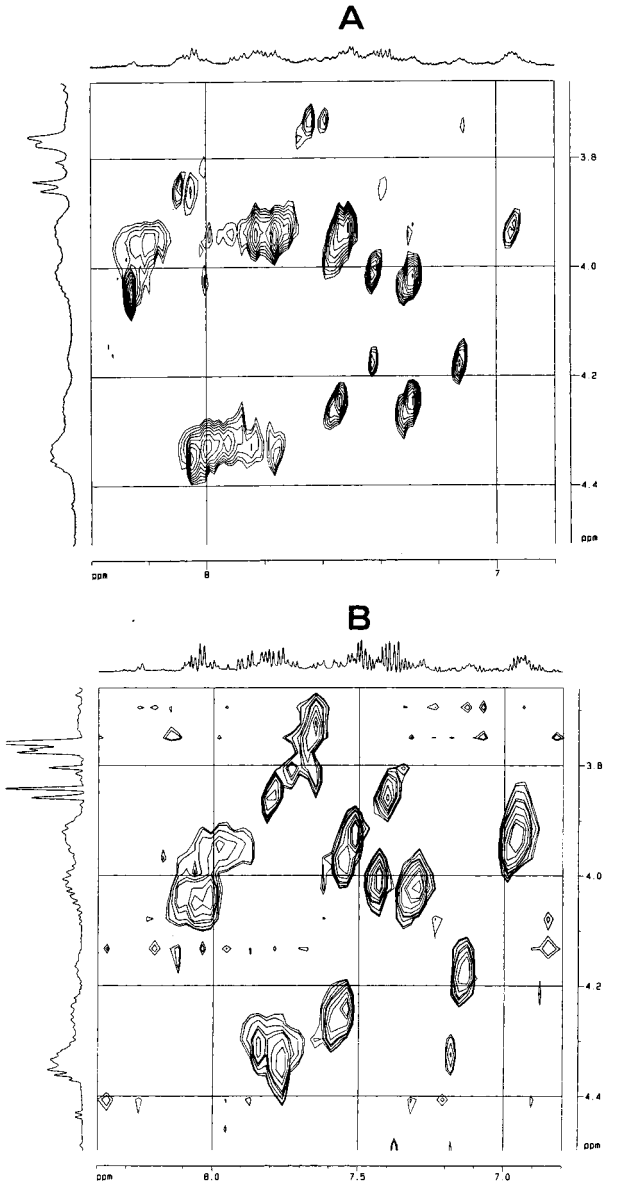

Figure 3. Particulars from the 2D maps. (A) Instructive slice of the NOESY spectrum. (B) Instructive slice of the corresponding TOCSY spectrum. Cross-peaks absent in part B and observable in part A are due to protons close in space but not belonging to the same residue.

$P(Aib)_2N$ is somewhat structured in DMSO solution. Additional contacts not listed in Table 1 are as follows: $d_{vin}-NH_{Leu^6}$ (strong), d_{vin}-$H^{\alpha}_{Leu^2}$ (weak), and $d_H\delta_{Lys^8}$-NH_{Lys^8} (medium), where *vin* denotes the vinyl group in the protoporphyrin IX. Interestingly, the latter contact should favor a hydrogen bond between the NH_{Lys^8} and the C=O group of the amide bond in the side chain carrying naphthalene.

Steady-State and Time-Resolved Emission Data. The steady-state fluorescence spectra of $P(Aib)_2N$ in different solvent media is illustrated in Figure 4 (λ_{ex} = 280 nm), where a substantial quenching of N singlet emission by the bound protoporphyrin can be noted in methanol and water/methanol 75/25 (v/v) but not in DMSO. Accordingly, the efficiency of the quenching process, E_N, as given by $[1 - (\Phi_{PN}/\Phi_N)]$, where Φ_{PN} is the peptide quantum yield, referred to naphthalene, and Φ_N is that of the blank carrying the N group only, is definitely lower in DMSO than in the other solvents, as shown in Table 2. By inspection of the table, it appears that E_N parallels with the efficiency of the

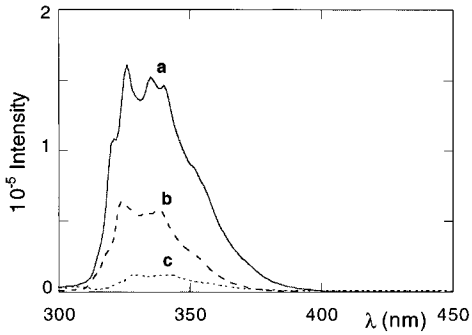

Figure 4. Fluorescence spectrum of $P(Aib)_2N$ in DMSO (a), CH_3OH (b), and H_2O/CH_3OH 75/25 (c); λ_{ex} = 280 nm. Minor exciplex emission occurs at around 420 nm in b and c but not in a, because only in the former solvents are the chromophores arranged in a parallel, almost face-to-face orientation.[3]

Table 2. Energy Transfer Efficiencies in Different Solvents, from Steady-State Measurements

solvent	E_N[a]	E_P[b]
DMSO	0.45	0.25
CH_3OH	0.81	0.81
H_2O/CH_3OH[c]	0.91	*d*

[a] λ_{ex} = 280. λ_{em} = 340 nm. $E_N = 1 - (\Phi_{PN}/\Phi_N)$. Φ_{PN} is the quantum yield of N* in $P(Aib)_2N$ and Φ_N = 0.22 that in $(Aib)_2N$. [b] λ_{ex} = 280. λ_{em} = 630 nm. $\Phi_N = [(I_{PN}/I_P) - 1](\epsilon_P C_P/\epsilon_N C_N)$, where $I_P = \epsilon_P C_P \Phi_P$ and $I_{PN} = \epsilon_P C_P \Phi_P + \epsilon_N C_N \Phi_P E_P$ are the fluorescence intensities of porphyrin in $(Aib)_2P$ and $P(Aib)_2N$, respectively, while C_P and C_N are the concentrations of the acceptor and donor chromophores. [c] 75/25 (v/v). [d] See ref 3.

fluorescence rise in P, E_P, thus indicating that the energy lost in the deactivation of the excited naphthyl chromophore is nearly completely transferred to the porphyryl group. This indicates that the N* quenching chiefly occurs by intramolecular $^1N^* \rightarrow P$ energy transfer in all solvents used.[2,3]

The modest N quenching observed in DMSO is suggestive of a rather large interchromophoric center-to-center distance or, possibly, a mutal orientation of the probes approaching 90°, provided that the donor and acceptor molecules do not rotate fast enough to randomize their orientation during the donor lifetime.[3]

We next investigated the fluorescence time decay of excited naphthalene in the same solvents. In all cases, no significant change was observed on varying sample concentration within one order of magnitude (2×10^{-6} to 2×10^{-5} M), which allows us to rule out interchain effects. The curves were well fitted by a two-component exponential decay; i.e.

$$I(t) = \sum_i \alpha_i \exp(-t/\tau_i) \qquad (1)$$

where i = 1 and 2, while the time decay of $(Aib)_2N$ was always found to be strictly monoexponential (e.g., τ_0 = 36.0 ± 0.9 ns in DMSO).

Whatever the solvent used, the shorter decay time, τ_1, is around 3 ns and is assigned to the energy transfer process, $^1N^* \rightarrow P$, in agreement with earlier results.[2,3] The longer decay time, τ_2, is around 45 ns in both methanol and water/methanol 75/25 (v/v) and measures a minor exciplex decay.[3] By contrast, it is around 38 ns in DMSO, being thus very similar to that observed for the unperturbed N* decay. Therefore, it can be reasonably assigned to this latter process, which is suggestive of a poor interaction and hence a rather large separation distance between N and P groups. Alterna-

Table 3. Fluorescence Time Decays of P(Aib)$_2$N in Different Solvents[a]

solvent	α_1	τ_1 (ns)	α_2	τ_2 (ns)	χ^2	E_1[b]
DMSO	0.37	2.6	0.63	37.6	1.0	0.93
CH_3OH	0.96	4.1	0.04	45.0	1.8	0.92
H_2O/CH_3OH[c]	0.96	2.5	0.04	45.5	1.3	0.93

[a] $\lambda_{ex} = 290$. $\lambda_{em} = 340$ nm. The time decay of N* in (Aib)$_2$N (blank) is $\tau_0 = 36.0 \pm 0.9$ ns (DMSO), 52.5 ± 1.5 ns (CH_3OH), and 36.2 ± 1.6 ns (H_2O/CH_3OH). The lifetime uncertainty is better than 5%, and that of the preexponents is around 20%. [b] Energy transfer efficiency, from eq 2. The uncertainty is better than 10%. [c] 75/25 (v/v).

tively, even though the probes are close to each other, this result may be due to a perpendicular mutual orientation of the probes, which prevents energy transfer from occurring if they are frozen on the time scale of the donor lifetime, as already mentioned.[3] In fact, energy transfer can take place when two conditions are matched. The first is a spectral requirement; i.e., the emission spectrum of the donor must overlap with the absorption spectrum of the acceptor. The second is a geometric requirement; i.e., the emission and absorption dipoles of the donor and acceptor molecules, respectively, must be at a certain distance and properly oriented, but perpendicularly.

The lifetimes and preexponents are reported in Table 3, together with the energy transfer efficiencies, as given by eq 2.

$$E_1 = 1 - (\tau_1/\tau_0) \tag{2}$$

Inspection of Table 3 shows that the preexponents also vary upon changing the solvent. For instance, in DMSO α_1 is around 0.4 as compared to a value around 0.9 in methanol or water/methanol 75/25. This indicates a variation in the population distribution of molecules undergoing the decay processes, which is not surprising for two reasons. Firstly, DMSO differs from methanol and the water/methanol mixture in both polarity and relaxation behavior.[12] Secondly, in methanol and water/methanol 75/25 the N and P groups are arranged in a parallel, almost face-to-face orientation.[3] Instead, the destructuring effects of DMSO are reflected not only in the backbone conformation but also in the spatial arrangement of the chromophore linkages, as shall be illustrated below.

Quantitatively, interprobe distances are commonly evaluated by eq 3 when both distance distributions and orbital overlap of the chromophores can be ignored. It gives the dependence of transfer efficiency on the inverse sixth power of the interprobe distance R. R_0 represents the distance at which 50% of the excitation energy is transferred,[13] and is given by eq 4,[14,15] where n is the refractive index, Φ_N is the donor fluorescence quantum yield in the absence of transfer, and J is the overlap integral, as given by eq 5.

$$E = R_0^6/(R_0^6 + R^6) \tag{3}$$

In eq 5, $\epsilon_A(\lambda)$ ($M^{-1}\cdot cm^{-1}$) is the extinction coefficient of the acceptor and $F_D(\lambda)$ is the corrected fluorescence emission spectrum of the donor, the spectral distribution of donor fluorescence being normalized to unity.

$$R_0 = (9.79 \times 10^3)[(^2/_3\Phi_N J)/n^4]^{1/6} \tag{4}$$

$$J = \frac{\int_0^\infty F_D(\lambda)\,\epsilon_A(\lambda)\lambda^4\,d\lambda}{\int_0^\infty F_D(\lambda)\,d\lambda} \tag{5}$$

From the spectral patterns, the overlap integral in DMSO is 5.18×10^{-14} $M^{-1}\cdot cm^3$ and hence R_0 is 31.4 Å.

The factor $^2/_3$ in eq 4 is the isotropic average value of the orientation parameter k^2, which is used when the chromophores are freely rotating.[16,17] In contrast, when the donor and acceptor molecules do not rotate fast enough to randomize their orientations during the donor lifetime, the orientation parameter is given by eq 6.[15] In such a case, a particular relative orientation between the probes is described by two angles only, γ and θ, where $0 \le \gamma$ and $\theta \le \pi$, the scheme for evaluating the orientation in space of the transition dipole moments of N* and P being already reported.[3]

$$k^2 = \cos^2\theta(3\cos^2\gamma + 1) \tag{6}$$

Molecular Modeling. Determination of conformations in solution by NMR is often made difficult by the large conformational changes occurring rapidly on the NMR time scale. The NMR observables and the restraints developed from them are consistent with an average structure that may not even exist.[18] Computational methods must assume, therefore, that the experimental observables arise from ensembles of conformers.[19] Accordingly, we have evaluated the most relevant structural features of the families of P(Aib)$_2$N conformers in DMSO by molecular mechanics calculations, making use of both NMR and fluorescence results as restraints.

The total energy for the mth conformer was evaluated by eq 7,[20] comprising stretching and bending terms (STR and BEN), besides nonbonding (NB), electrostatic (COUL), and torsional (TOR) potentials similar to those previously employed by us.[2,3,21]

$$U_{m,tot} = NB + COUL + TOR + STR + BEN \tag{7}$$

Even though computational data on flexible molecules must be taken with some caution, the use of eq 8 overcomes the uncertainty in the absolute value of the total energy, arising from the empirical terms of eq 7. In fact, ΔU_{tot} is the difference between the total energy of the mth conformer, $U_{m,tot}$, and the lowest energy among all conformers of the peptide, U_{min}. In addition, the experimental restraints used give further confidence in the computational results.

$$\Delta U_{tot} = U_{m,tot} - U_{min} \tag{8}$$

Briefly, the long range NOE contacts, shown in Figure 5, as well as both the NOE contacts and the $J_N\alpha_H$ values reported in Table 1, were used as restraints for computing the molecular models, together with both the interprobe distance and the k^2 parameter (eqs 3 and 6), as obtained by fluorescence decay experiments. Energy minimization was then carried out in the multidimensional space of the internal rotation angles, making use of the Karplus−Pardi expression (eq 9)[22] when appropriate, and employing the R_m and k_m^2 values for optimizing the agreement between calculated (eq 10) and experimental (eq 2) energy transfer efficiencies of the mth conformer, R_m and k_m^2 being the interprobe distance and orientation parameter, respectively.

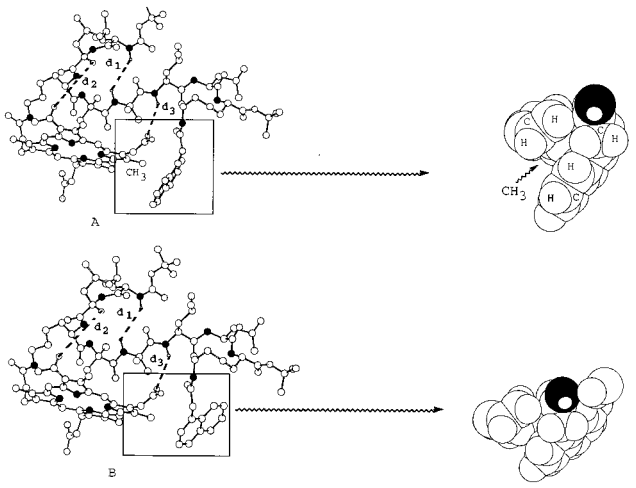

Figure 5. Molecular models of the sterically most favorable conformers pertaining to one family of P(Aib)$_2$N in DMSO. The molecular parameters and energies are listed in Table 4. Nitrogen atoms are in black, and hydrogen atoms are omitted for clarity. Broken lines indicate the long range NOE contacts, corresponding to the following distances: $d_1 = 3.291$ Å, $d_2 = 5.071$ Å, $d_3 = 3.035$ Å (A); $d_1 = 3.301$ Å, $d_2 = 5.019$ Å, $d_3 = 2.862$ Å (B). The space-filled model of both naphthalene and the neighboring porphyrin CH_3 group on the right side of the figure shows how good are the nonbonding contacts between the two moieties. They are partly responsible for the freezing of the N and P chromophores in a perpendicular mutual orientation, which prevents energy transfer from occurring (see text).

$$J_N\alpha_H = 6.7\cos^2(\phi - 60) - 1.3\cos(\phi - 60) + 1.5 \quad (9)$$

$$E_m = \frac{1}{1 + \left[\frac{2}{3k_m^2}\left(\frac{R_m}{R_0}\right)^6\right]} \quad (10)$$

Where the average transfer efficiency of the conformers within each family was needed, eq 11 could be used, where the sum is taken over all conformers and P_m' is the corresponding probability, within the same family.

$$\langle E\rangle = \sum E_m \cdot P_m' \quad (11)$$

Details of calculations shall be reported elsewhere, while the most relevant results may be summarized as follows. (1) The sterically most favorable conformers of P(Aib)$_2$N in DMSO pertain to two families. They differ from each other for both the interprobe separation distance and mutual orientation, and for their internal mobility as well. (2) One family comprises two sterically favored conformers, denoted as **A** and **B**, whose molecular parameters and relative energies are listed in Table 4. The molecular models, illustrated in Figure 5, show how the molecules fold around the Aib residues, in agreement with the long range NOE contacts, giving rise to a β-turn-like arrangement. Moreover, by using the fluorescence decay data as restraints in the energy minimization, it turns out that the chromophores are close to each other, the average interprobe distance being $\langle R\rangle = 9.3$ Å, and exhibit a perpendicular orientation. The proximity of P and N groups optimizes their van der Waals contacts, as clearly shown by the space-filled models illustrated in the same figure, while short range porphyrin−backbone interactions stiffen this part of the molecule. As a result, the internal rotation of the chromophores is frozen on the time scale of the transfer process, so that the perpendicular orientation of the probes prevents energy transfer from occurring.[3] This agrees with the observation that the long lifetime, τ_2, measures the decay of the unperturbed singlet naphthalene only (Table 3). Collisions with solvent molecules in solution are likely to provide energy for librational motions of naphthalene around its equilibrium position, though the perpendicular arrangement of the probes should be, on the average, maintained because librations are definitely faster than energy transfer. (3) Computational results are further supported by the finding that the calculated population of this family (Table 4) satisfactorily compares, in view of the approximations made, with that experimentally determined, as given by the α_2 preexponent (Table 3). (4) The other family comprises six sterically favored conformers, denoted as **C**−**H** in Table 4, where their molecular parameters and energies are listed, and in Figure 6, where the representative structures **C** and **H** are shown. These are quickly interconverting conformers on the time scale of the energy transfer, in agreement with the distribution analysis of time decays in DMSO, exhibiting a single peak centered at 3 ± 0.3 ns (Figure 7), besides the peak at around 38 ns due to the N* decay (not shown).

By inspection of Figure 6, it clearly appears that the β-turn-like arrangement around the Aib residues is preserved, while intramolecular hydrogen bonds between NH_{Lys1} and CO_{Aib5}, and NH_{Lys8} and ϵ-CO of Lys[8]

Table 4. Molecular Parameters and Energies of P(Aib)$_2$N Conformers in DMSO, As Obtained by Molecular Mechanics Calculations Restrained by NMR and Fluorescence Data[a]

conformer	k_m^2 [b]	R_m [c]	E_m [d]	ΔU_{tot} [e]	P_m [f]
A	≈0	9.93	≈0	0	0.29
B	≈0	8.71	≈0	1.1	0.04
C	0.60	18.60	0.954	0.5	0.13
D	0.56	18.71	0.940	1.0	0.04
E	0.60	17.78	0.964	0.7	0.10
F	0.71	18.67	0.958	0.5	0.12
G	0.62	19.21	0.946	1.2	0.04
H	0.62	19.35	0.942	0.1	0.24
average	0.63 ± 0.05	18.7 ± 0.4	0.95 ± 0.1[g]		

[a] The sterically most favorable conformers pertain to two families: one comprises **A** and **B**, and the other **C**, **D**, **E**, **F**, **G** and **H**. [b] Orientation parameter of the probes in the mth conformer; $k^2 = 0$ arises from the chromophores frozen in a strictly perpendicular orientation (see text). [c] Calculated interprobe center-to-center distance in the mth confomer (Å). [d] Calculated energy transfer efficiency in the mth conformer, as obtained by eq 10 using the computed values of R_m and k_m^2. [e] In kcal·mol^{-1}, from eq 8, where U_{min} refers to conformer **A**. [f] Probability of the mth conformer, $P_m = \exp(-\Delta U_{tot}/RT)/\sum\exp(-\Delta U_{tot}/RT)$, the sum being over all conformers. [g] To be compared with the experimental E_1 value reported in Table 3.

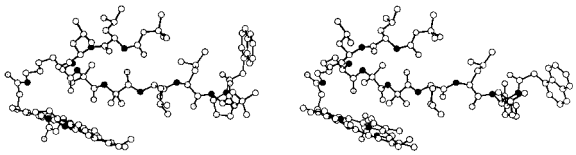

Figure 6. Representative structures of the quickly interconverting conformers on the time scale of energy transfer, pertaining to the other family of P(Aib)$_2$N in DMSO. The average values of the molecular parameters are reported in Table 4. Nitrogen atoms are in black, and hydrogen atoms are omitted for clarity. The average mutual orientation of the probes is such as to allow energy transfer to occur, despite the rather large interprobe center-to-center distance ($\langle R\rangle = 19$ Å).

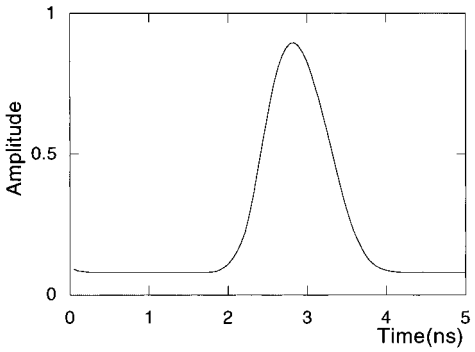

Figure 7. Population distribution from time decay measurements of $P(Aib)_2N$ in DMSO. Only the first peak, centered at 3 ± 0.3 ns, is shown, measuring the energy transfer. The other peak is centered at around 38 ns and is due to the unperturbed naphthalene decay.

further stiffen this part of the molecule. However, the N group is now lying far away from protoporphyrin. In addition, the average value of the orientation parameter necessary for a satisfactory agreement between calculated and experimental transfer efficiencies is $\langle k^2 \rangle = 0.63 \pm 0.05$, as reported in Table 4. This value is very close to the "dynamic" isotropic average of the orientation parameter, i.e. $\langle k^2 \rangle = {}^2/_3$, which strongly suggests that this time the N group freely rotates on the time scale of the transfer process, in full agreement with the result of Figure 7.

Concluding Remarks

Combination of NMR with fluorescence data was productive in determining the structural features of $P(Aib)_2N$ conformers in DMSO. In all cases, the molecules fold around the Aib residues, assuming a β-turn-like arrangement, which is stabilized by short range interactions within the backbone chain, as well as between the backbone and the protoporphyrin group. The structural features of the other (unfolded) part of the molecules depend on whether the naphthyl moiety is close to protoporphyrin or far away from it, the average center-to-center distance changing from about 9 to 19 Å, respectively. In the former case, the chromophores are frozen in a perpendicular orientation, which prevents energy transfer from occurring despite their proximity. In the latter case, the naphthyl moiety is freely rotating, being thus able to assume an average isotropic orientation with respect to the P group, the characteristic time for the internal rotation of N being shorter than that of the transfer process (3 ns).

Acknowledgment. We wish to thank Dr. G. Zanotti for the generous gift of the samples, and the National Research Council (C. N. R.) for the financial support.

References and Notes

(1) Houston, M. E., Jr.; Gannon, C. L.; Kay, C. M.; Hodges, R. S. *J. Pept. Sci.* **1995**, *1*, 274.
(2) Pispisa, B.; Venanzi, M.; Palleschi, A.; Zanotti, G. *J. Mol. Liquids* **1994**, *61*, 167; *Macromolecules* **1994**, *27*, 7800; *Biopolymers* **1994**, *36*, 497.
(3) Pispisa, B.; Palleschi, A.; Venanzi, M.; Zanotti, G. *J. Phys. Chem.* **1996**, *100*, 6835.
(4) Basu, G.; Bagchi, K.; Kuki, A. *Biopolymers* **1991**, *31*, 1763.
(5) Aue, W. P.; Bartholdi, E.; Ernst, R. R. *J. Chem. Phys.* **1976**, *64*, 2229.
(6) Braunschweiler, L.; Ernst, R. R. *J. Magn. Reson.* **1983**, *53*, 521.
(7) Jeener, J.; Meier, B. H.; Bachmann, P.; Ernst, R. R. *J. Chem. Phys.* **1979**, *71*, 4546.
(8) Marion, D.; Wütrich, K. *Biochem. Biophys. Res. Commun.* **1983**, *113*, 967.
(9) Bax, A.; Davis, D. G. *J. Magn. Reson.* **1985**, *65*, 355.
(10) Natgayama, K.; Wütrich, K. *Eur. J. Biochem.* **1981**, *114*, 365.
(11) Wütrich, K. *NMR in Biological Research. Peptides and Proteins*; North-Holland: Amsterdam, 1976; chapter 3, p 74 and references therein.
(12) Simon, J. D. *Acc. Chem. Res.* **1988**, *21*, 128. Weaver, M. J.; McManis, G. E., III. *Acc. Chem. Res.* **1990**, *23*, 294.
(13) Cheung, H. C. In *Topics in Fluorescence Spectroscopy*; Lakowicz, J. R., Ed.; Plenum Press: New York, 1991; Vol. 2, Chapter 3.
(14) Förster, T. *Ann. Phys. (Leipzig)* **1948**, *2*, 55; *Discuss. Faraday Soc.* **1959**, *27*, 7.
(15) Steinberg, I. Z. *J. Chem. Phys.* **1968**, *48*, 2411. Grinvald, A.; Haas, E.; Steinberg, I. Z. *Proc. Natl. Acad. Sci. U.S.A.* **1972**, *69*, 2273.
(16) Valeur, B.; Mugnier, J.; Pouget, J.; Bourson, J.; Santi, F. *J. Phys. Chem.* **1989**, *93*, 6073. Inai, Y.; Sisido, M.; Imanishi, Y. *J. Phys. Chem.* **1990**, *94*, 6237.
(17) McWherter, C. A.; Haas, E.; Leed, A. R.; Scheraga, H. A. *Biochemistry* **1986**, *25*, 1951.
(18) Mierke, D. F.; Kurz, M.; Kessler, H. *J. Am. Chem. Soc.* **1994**, *116*, 1042.
(19) Landis, C.; Allured, V. S. *J. Am. Chem. Soc.* **1991**, *113*, 9493. Kenmink, J.; van Mierlo, C. P. M.; Scheek, R. M.; Creighton, T. E. *J. Mol. Biol.* **1993**, *230*, 312.
(20) Pispisa, B.; Palleschi, A.; Venanzi, M.; Zanotti, G. *J. Photochem. Photobiol., A*, in press.
(21) Pispisa, B.; Palleschi, A.; Barteri, M.; Nardini, S. *J. Phys. Chem.* **1985**, *89*, 1767. Pispisa, B.; Palleschi, A.; Paradossi, G. *J. Phys. Chem.* **1987**, *91*, 1546. Pispisa, B.; Paradossi, G.; Palleschi, A.; Desideri, A. *J. Phys. Chem.* **1988**, *92*, 3422. Paradossi, G.; Chiessi, E.; Venanzi, M.; Pispisa, B.; Palleschi, A. *Int. J. Biol. Macromol.* **1992**, *14*, 73. Chiessi, E.; Branca, M.; Palleschi, A.; Pispisa, B. *Inorg. Chem.* **1995**, *34*, 2600.
(22) Ludvigsen, S.; Andersen, K. V.; Poulsen, F. M. *J. Mol. Biol.* **1991**, *217*, 731 and references therein.

MA9618336